

Photorealistic rendering of a graded negative-index metamaterial magnifier

This article has been downloaded from IOPscience. Please scroll down to see the full text article.

2012 New J. Phys. 14 033024

(<http://iopscience.iop.org/1367-2630/14/3/033024>)

View [the table of contents for this issue](#), or go to the [journal homepage](#) for more

Download details:

IP Address: 137.132.3.10

The article was downloaded on 15/03/2012 at 02:19

Please note that [terms and conditions apply](#).

Photorealistic rendering of a graded negative-index metamaterial magnifier

Cheng-Wei Qiu¹, Alireza Akbarzadeh, Tiancheng Han
and Aaron J Danner

Department of Electrical and Computer Engineering, National University of
Singapore, Kent Ridge, Singapore 119620, Republic of Singapore
E-mail: eleqc@nus.edu.sg

New Journal of Physics **14** (2012) 033024 (10pp)

Received 11 December 2011

Published 14 March 2012

Online at <http://www.njp.org/>

doi:10.1088/1367-2630/14/3/033024

Abstract. A novel reverse design schematic for designing a metamaterial magnifier with graded negative refractive index for both the two-dimensional and three-dimensional cases has been proposed. Photorealistic rendering is integrated with trace ray trajectories in example designs to visualize the scattering magnification as well as imaging of the proposed graded-index magnifier with negative-index metamaterials. The material of the magnifying shell can be uniquely and independently determined without knowing beforehand the corresponding domain deformation. This reverse recipe and photorealistic rendering directly tackles the significance of all possible parametric profiles and demonstrates the performance of the device in a realistic scene, which provides a scheme to design, select and evaluate a metamaterial magnifier.

 Online supplementary data available from stacks.iop.org/NJP/14/033024/mmedia

Contents

1. Introduction	2
2. Two-dimensional design	3
3. Three-dimensional design	6
4. Conclusion	9
Acknowledgments	10
References	10

¹ Author to whom any correspondence should be addressed.

1. Introduction

Conformal mapping [1] and coordinate transformations [2] have been developed to derive the required parameters in optical instruments with pre-defined functionality. These methods pave an unprecedented avenue to various conceptual devices that possess exotic control over the propagation of electromagnetic (EM) waves. Among those rational designs with novel manipulation of EM waves, cloaking, which makes objects invisible, has been attracting increasing attention, especially because metamaterials are found to be a potential candidate to realize the cloaks [3]. Practical attempts to realize a cylindrical cloak have been made in the microwave [4] and optical [5] regimes. The coordinate transformation employed relies on the invariance of Maxwell's equations throughout the spatial transformation. A variety of applications have been studied such as carpet cloaks [6], external cloaks [7], superscattering and shifting effects [8], beam splitters [9], homogeneous nonmagnetic bends [10] and field collimators [11], which have been reviewed in [12]. Instead of cloaking an object (i.e. shrinking the scattering cross section of the object), a magnifier is of great interest to the scientific community in the other extreme. The magnifier could form an image exceeding the physical size of the object. Transformation optics have been applied to design cylindrical superscatters [13], and the concept of complementary illusion optics has been used in conjunction with a transmission line circuit to achieve superscattering [14], although the enlargement of scattering cross section is mimicked by the voltage measured on the circuit board. Graded-index materials derived from transformation optics have been used in [15] to magnify subwavelength features of an object for the purpose of super-resolution, although only a virtual image rather than a real image can be provided via the proposed method. As has been addressed in [16], practical limitations of dissipation and loss upon realizing cloaks need to be considered in fabrication. In this respect, more recently, low-loss dielectric cloaks have been fabricated by the use of calcites, which further overcomes the loss problem [17].

Nevertheless, previous transformation-optic methods require knowledge of the spatial transformation first, so as to derive the corresponding parameters for simulations and experiments. In our reverse design of the two-dimensional (2D) and three-dimensional (3D) metamaterial magnifiers, there is, by the nature of the space compression, an infinite number of possible transformation functions, all of which can lead to identical magnifying functionality. However, because of practical limitations of fabrication and consideration of the cost, it is better to wisely select a model which has less stringent parameters and/or is easier to realize by current fabrication techniques. It is due to the fact that the metamaterial technology, although developing fast, is still far from being capable enough to produce stealth aircraft or optical cloak/camouflage perfectly in action. Hence, it is useful to directly envisage the desired parameters of the metamaterial magnifier (i.e. impose the explicit final parameters first), since complexity and feasibility are predetermined and the photorealistic rendering will further facilitate seeing how those conceptual devices will behave in the practical outdoor environment and to the best of today's and futuristic materials. In contrast to usual methods (i.e. knowing a class of transformation functions and then determining the final parameters), we actually flip the design sequence by presenting a reverse methodology to determine the required parameters of a magnifier, without knowing the specific coordinate transformation beforehand. By directly analyzing the parameters and examining whether there is a physical solution to the transformation function, our approach provides a robust tool to evaluate if metamaterial magnifiers can be accessible and simplified in terms of homogeneity, isotropy, non-singularity, etc. Accordingly,

different designs will be examined and eventually their advantages and disadvantages will be shown. In addition to geometric raytracing, photorealistic raytracing [18] has been used to evaluate grating cloaks. We will employ the photorealistic rendering technique to visualize the scattering magnification and the imaging properties by tracing ray trajectories and also simulate how such a device behaves in a real environment before it is built.

The advantage of this reverse transformation method is threefold: (i) a *generating function* together with the boundary conditions, in fact, replaces the corresponding spatial deformation; instead of considering the coordinate transformation directly, the reverse mechanism enables us to easily derive different parametric profiles by selecting such a generating function, e.g. exponential, Gaussian, quadratic, etc; thus all possible types of magnifiers can be explored robustly. (ii) From the parameters obtained in such a reverse method, it is easier to manipulate the material properties (e.g. isotropy, non-singularity and homogeneity), and finally one can determine a particular generating function $g(r)$ that gives rise to an isotropic and nonsingular scattering magnifier by the use of graded negative-index materials. (iii) Other optical devices that lead to interesting phenomena such as super-resolution imaging and perfect lens can be designed since the feature image can be greatly enlarged; the proposed integrated recipe provides insightful access to parameter simplification (e.g. removal of anisotropy, singularity or inhomogeneity), and to the real-life emulation of perfection or imperfection in the device before being built. This reverse design still relies on negative-index materials, even though non-singularity can be avoided and the inhomogeneity in certain material parameters can be much alleviated. Nevertheless, the reverse design method sheds some light on how to robustly select a more suitable set of material parameters, and the advanced photorealistic rendering enables us to perceive and visualize the device performance in the presence of material imperfection beforehand due to the fabrication limit.

2. Two-dimensional design

First, let us assume that a circular region ($r \leq a$) covered by complementary media ($a \leq r \leq b$) in physical space $\Omega(r)$ is transformed from a circular region ($r' \leq c$) in virtual space $\Omega'(r')$ via an *unknown* transformation function. The complementary media are assumed to be equal for impedance matching, i.e. $\bar{\epsilon}(r) = \bar{\mu}(r) = \alpha_r \hat{r}\hat{r} + \alpha_\theta \hat{\theta}\hat{\theta} + \alpha_z \hat{z}\hat{z}$. The geometry is folded along the radial direction, and thus the Jacobian matrix is diagonal, although we still have no information on what the coordinate transformation is. The relative parameters of the complementary media can be obtained: $\bar{\epsilon} = \bar{\mu} = \bar{A} \cdot \bar{A}^{-T} / \det(\bar{A})$ [1, 2], where $\bar{A} = \partial(r, \theta, z) / \partial(r', \theta', z')$ is the Jacobian matrix, and (r', θ', z') and (r, θ, z) represent the EM space and the physical space, respectively. Then, three principal values of $\bar{\epsilon}(r)$ and $\bar{\mu}(r)$ can be derived: $\alpha_r = \frac{r' dr'}{r dr}$, $\alpha_\theta = \frac{1}{\alpha_r}$ and $\alpha_z = \frac{r' dr'}{r dr}$. By making use of the identities $\alpha_r \alpha_z = (r'/r)^2$ and $r \sqrt{\alpha_r \alpha_z} \partial[r \sqrt{\alpha_r \alpha_z}] / \partial r = r \alpha_z$, one can obtain

$$r'^2 = C_0 + 2 \int_a^r r_1 \alpha_z(r_1) dr_1, \quad (1)$$

where C_0 is a constant. Due to the folding configuration ($r' = c$ when $r = a$), we have $C_0 = c^2$ from equation (1). Another condition ($r' = b$ when $r = b$) leads to the normalization

$$\int_a^b r_1 \alpha_z(r_1) dr_1 = \frac{b^2 - c^2}{2}. \quad (2)$$

Here, we introduce the generating function $g(r)$ which is proportional to $\alpha_z(r)$, i.e. $\alpha_z(r) = d_0 g(r)$, where d_0 is an arbitrary constant. Substituting $\alpha_z(r) = d_0 g(r)$ into equation (2), we can obtain $d_0 = (b^2 - c^2) / [2 \int_a^b r_1 g(r_1) dr_1]$. Thus $\alpha_z(r)$ can be expressed as

$$\alpha_z(r) = \frac{(b^2 - c^2)g(r)}{2 \int_a^b r_1 g(r_1) dr_1}. \quad (3)$$

From the aforementioned identity $\alpha_r \alpha_z = (r'/r)^2$ and equation (3), $\alpha_r(r)$ can be determined:

$$\alpha_r(r) = \frac{c^2 + 2 \int_a^r r_1 \alpha_z(r_1) dr_1}{r^2 \alpha_z(r)}. \quad (4)$$

The unknown coordinate transformation for the corresponding complementary media can, in turn, be found.

$$r' = \sqrt{c^2 + 2 \int_a^r r_1 \alpha_z(r_1) dr_1}. \quad (5)$$

To validate this method, we select a specific generating function as the representative demonstration, i.e. $g(r) = r^n$ ($n = 0, \pm 1, \pm 2, \dots$). Then $\alpha_z(r)$ can be derived.

$$\begin{aligned} \alpha_z(r) &= \frac{(n+2)(b^2 - c^2)r^n}{2(b^{n+2} - a^{n+2})} \quad \text{when } n \neq -2, \\ \alpha_z(r) &= \frac{b^2 - c^2}{2r^2 \ln(b/a)} \quad \text{when } n = -2. \end{aligned} \quad (6)$$

Its corresponding coordinate transformation can be expressed as

$$\begin{aligned} r' &= \sqrt{c^2 + \frac{(b^2 - c^2)(r^{n+2} - a^{n+2})}{b^{n+2} - a^{n+2}}} \quad \text{when } n \neq -2, \\ r' &= \sqrt{c^2 + \frac{(b^2 - c^2) \ln(r/a)}{\ln(b/a)}} \quad \text{when } n = -2. \end{aligned} \quad (7)$$

Reverse magnifiers designed with generating functions corresponding to different values of n are presented for $g(r) = 1/r^2$ (i.e. $n = -2$), $g(r) = 1/r^{10}$ (i.e. $n = -10$) and $g(r) = r^{10}$ (i.e. $n = 10$) in figures 1(b)–(d). It can be found that the electric fields for those three types are equivalent outside the black dashed lines ($r > c$), where the scattering pattern of a small circular perfect electric conductor (PEC) ($r = a$) covered by complementary media is equivalent to that of the bare PEC ($r = c$) in figure 1(a).

Figure 1(d) reveals that the generating function $n = 10$, compared to the other two cases, gives rise to the smallest scattering intensity in the complementary media, and the area of white flecks is also minimal and confined just near the outer boundary ($r = b$). It can be explained that the implied spatial transformation corresponding to the case of the generating function $n = 10$ will fold and compress more virtual space into the area near the outer boundary in physical space, which can be verified by plotting equation (7) for $n = 10$. It is worth noting that those high-intensity areas are always associated with high heat generation, which is a big problem in real applications. One potential solution for solving such a heat problem could be to mount a cooling fin externally since the high-field-intensity region is pushed to the outer boundary.

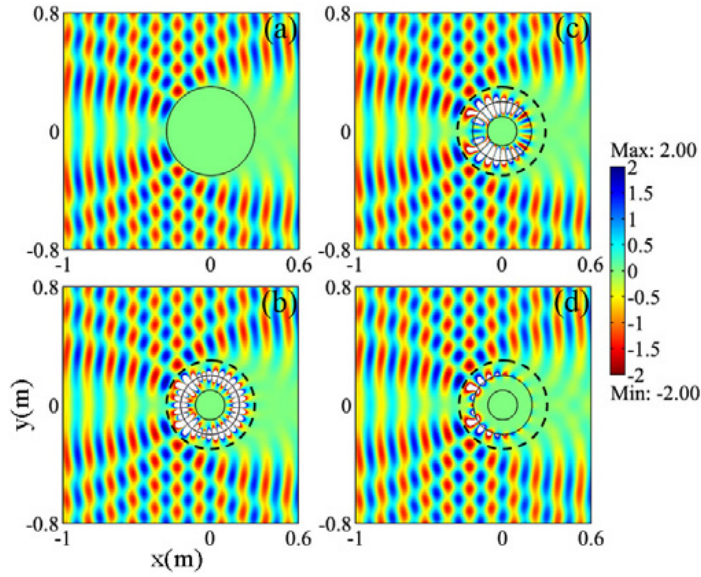


Figure 1. Snapshots of the total electric field for the reverse designed superscattering magnifier. (a) A bare PEC cylinder with radius c . (b) $n = -2$; (c) $n = -10$; (d) $n = 10$. Note that $a = 0.1$ m, $b = 2a$ and $c = 3a$.

This reverse recipe can thus be a powerful tool to design isotropic and nonsingular magnifiers with retro-reflecting and imaging features by the use of graded negative refractive index. From the condition $\alpha_\theta = 1/\alpha_r$, the isotropy imposes that $\alpha_r = \pm 1$ in equation (4). By taking the derivative of $\pm r^2 \alpha_z(r) = c^2 + 2 \int_a^r r_1 \alpha_z(r_1) dr_1$, one thus has $g(r) = T$ (T is a constant) or $r^2 g'(r) + 4r g(r) = 0$, respectively. The following shows the design analysis.

1. In the case of $g(r) = T$ corresponding to $\alpha_r = 1$, the isotropy (under one polarization) implies $T d_0 = c^2/a^2$. However, the aforementioned normalization $d_0 = (b^2 - c^2)/[2 \int_a^b r_1 g(r_1) dr_1]$ implies $T d_0 = (b^2 - c^2)/(b^2 - a^2)$, which is contradictory. Hence, $g(r) = T$ is not possible for isotropic designs.
2. In the case of $r^2 g'(r) + 4r g(r) = 0$ corresponding to $\alpha_r = -1$, the generating function becomes $g(r) = 1/r^4$. After solving for the normalization, it is found that only when $c = b^2/a$ can one obtain isotropic complementary media $\alpha_r = \alpha_\theta = -1$ and $\alpha_z(r) = -b^4/r^4$. Therefore, an isotropic negative-index magnifier can be realized for one polarization, e.g. $\epsilon = -1$ and $\mu = -b^4/r^4$ for transverse magnetic (TM) incidence and $\epsilon = -b^4/r^4$ and $\mu = -1$ for transverse electric (TE) incidence. The isotropic design derived from the reverse method is thus in agreement with the corresponding result in [7].

It is worth noting that the cases above only depend on nonsingular parameters ($a < r < b$).

To emulate how such an isotropic design (i.e. Point 2) behaves in practice, a raytracing (photorealistic) technique has been developed. Photorealistic raytracing can also help quantitatively foresee how a specific imperfection in materials will affect the device performance, although in this paper we use it only to visualize the ideal performance. Figure 2(a) indicates that upper and lower rays intersect each other twice in the vicinity of the outer boundary $r = b$ owing to the negative refractive index in the transverse plane of the isotropic shell. Figure 2(b) demonstrates the imaging properties in which only the images before and after

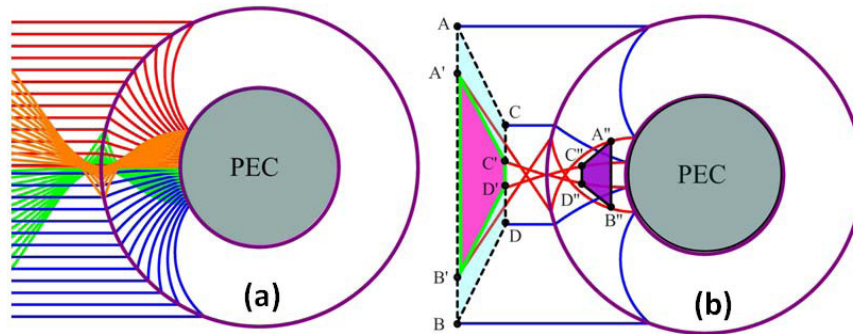


Figure 2. Raytracing of the isotropic negative-index shell whose parameters are $\varepsilon = -b^4/r^4$ and $\mu = -1$. (a) Ray trajectories for light before hitting the PEC (red and blue), after being reflected by the PEC (orange and green); red and orange lines correspond to rays in the upper-half space; blue and green lines correspond to the rays in the lower half. (b) The images inside the isotropic shell and outside the isotropic shell. Note that $a = 0.2$ m, $b = 2a$ and $c = b^2/a$. A photorealistic rendering of such an isotropic magnifier is shown in movie 1 (available from stacks.iop.org/NJP/14/033024/mmedia), where b is fixed at 0.2 m and a is varying up to 0.2 m (i.e. $c = b$, no magnification).

ray intersection areas are shown. It reveals that the image inside the isotropic shell (A''B''C''D'') is flipped (left-side right) and the image outside the shell (A'B'C'D') is preserved, while both have their shapes deformed. Hence the image outside the isotropic shell will not be inverted, in contrast to the Eaton lens flipping the image upside down [19].

In figure 3(a), a bare PEC rod ($r < b$) is placed in the waveguide, so the wave will certainly be partially transmitted via the openings between the PEC rod and the waveguide walls, as shown in figure 3(c). However, in figure 3(b), when a smaller PEC rod ($r < a$) is coated by an isotropic shell ($a < r < b$), the coated rod effectively behaves as a magnified PEC rod ($r = 0.04$ m). Therefore, even though the coated structure in figure 3(b) has its outermost radius physically identical to that in figure 3(a), the PEC in figure 3(b) will be magnified and block the whole waveguide width (since the width of the waveguide is 0.08 m). This is verified from the field distribution in figure 3(b) and the transmission spectra in figure 3(c).

3. Three-dimensional design

The reverse design scheme for 2D cases can also be extended to develop 3D magnifiers. Similar to the 2D case, a spherical region ($r \leq a$) covered by a metamaterial shell ($a \leq r \leq b$) in physical space $\Omega(r)$ can be transformed from a spherical region ($r' \leq c$) in virtual space $\Omega'(r')$ via an unknown transformation function.

The medium in the magnifying shell ($a \leq r \leq b$) has the following relative permittivity and permeability:

$$\varepsilon = \mu = \text{diag} \{ \xi_r, \xi_t, \xi_t \} = \text{diag} \{ \lambda_r / \lambda_t^2, 1 / \lambda_r, 1 / \lambda_r \}, \quad (8)$$

where $\lambda_r = dr/dr'$ and $\lambda_t = r/r'$. Since our shrinkage in the spherical coordinate system is in the radial direction, the transformation function is dependent only on r , i.e. $r' = U(r)$. Now, let

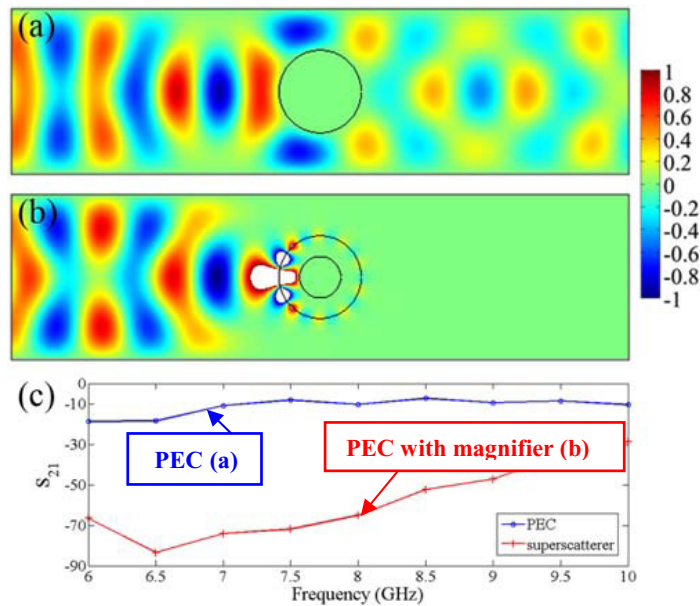


Figure 3. The width of the waveguide is 0.08 m, the simulation frequency is 8 GHz and the incident wave is TE polarized. (a) A snapshot of the magnetic field for a bare PEC cylinder (radius: $b = 0.02$ m) in the waveguide. (b) A snapshot of the magnetic field for a bare PEC cylinder (radius: $a = 0.01$ m) coated with an isotropic magnifying shell (outer radius: $b = 0.02$ m; refractive index: $n = -b^2/r^2$). (c) Transmission spectra for (a) and (b).

us choose $\xi_t(r) = A_0 g(r)$, where $g(r)$ can be any arbitrary well-defined function and A_0 is a constant. So we have

$$\xi_t(r) = \frac{dr'}{dr} = A_0 g(r). \quad (9)$$

If we solve for r' , we obtain

$$r' = U(r) = A_1 + A_0 \int_a^r g(\tau) d\tau. \quad (10)$$

Satisfying the boundary conditions $r'|_{r=a} = U(a) = c$ and $r'|_{r=b} = U(b) = b$, leads, respectively, to $A_1 = c$ and

$$A_0 = \frac{b - c}{\int_a^b g(\tau) d\tau}. \quad (11)$$

From equation (8), we know that

$$\xi_r(r)\xi_t(r) = \left(\frac{r'}{r}\right)^2. \quad (12)$$

Hence, from equations (9) and (11), we obtain

$$\xi_r(r) = \left(\frac{r'}{r}\right)^2 \frac{1}{A_0 g(r)} = \left(c + \frac{b - c}{\int_a^b g(\tau) d\tau} \int_a^r g(\tau) d\tau\right)^2 \frac{\int_a^b g(\tau) d\tau}{(b - c)r^2 g(r)}. \quad (13)$$

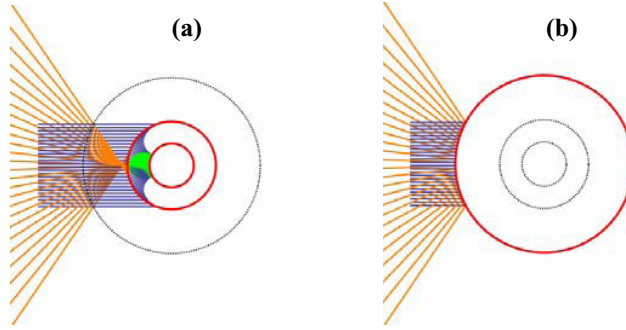


Figure 4. (a) Ray traces for a PEC sphere of radius a enclosed in a complementary medium with thickness of $b - a$ (solid red lines); (b) ray traces for a bare PEC sphere of radius c (solid red line). The blue and orange lines denote incident and scattered rays, respectively.

Now choosing $g(r) = r^n$ as an example, we find the corresponding transformation functions, $\xi_r(r)$ and $\xi_t(r)$, of the proposed spherical magnifier,

$$r' = U(r) = \frac{c(b^{n+1} - r^{n+1}) + b(r^{n+1} - a^{n+1})}{b^{n+1} - a^{n+1}}. \quad (14)$$

$$\xi_t(r) = -\frac{(n+1)(c-b)r^n}{b^{n+1} - a^{n+1}}. \quad (15)$$

$$\xi_r(r) = -\frac{(c(b^{n+1} - r^{n+1}) + b(r^{n+1} - a^{n+1}))^2}{(n+1)(c-b)(b^{n+1} - a^{n+1})r^{n+2}}. \quad (16)$$

Shown in figure 4(a) are the traces of rays impinging on the PEC small sphere of radius $a = 0.1$ m coated with the complementary medium $a \leq r \leq b = 2a$, while the paths of the rays scattered by a single PEC sphere of radius $c = b^2/a$ are presented in figure 4(b). Comparing figure 4(a) with figure 4(b) reveals that the scattered rays from the coated small sphere follow the same traces as the rays scattered from the bigger PEC sphere. It is interpreted that the scattering cross section of the small composite sphere is equal to that of the big PEC one. As mentioned earlier, there is no theoretical limit on a and c , which means that they can be as small or large as possible, although the coating medium profile might be mathematically complicated. Note that since our structure is spherically symmetric, the corresponding Hamiltonians of the TE and TM modes do not have any terms in common and therefore the designed structure can work for both TE and TM modes.

A photorealistic demonstration of the designed spherical magnifier is presented in figure 5. As can be seen in this figure, a small spherical mirror of radius $a = 0.1$ m with the annular coating with the outer boundary $b = 2a$ is compared with a non-coated single spherical mirror of radius $b = 2a$ in a photorealistic manner.

Both the spheres are actually placed in front of an infinitesimally small virtual camera, which is circumscribed by a background scene of a garden pictured panoramically in figure 5(a).



Figure 5. (a) Panoramic depiction of the background scene; (b) a snapshot of the magnified mirror; (c) a snapshot of the non-coated mirror. The physical size of (b) and (c) is the same. The animations for (b) and (c) are provided in movies 2 and 3 (available from stacks.iop.org/NJP/14/033024/mmedia), respectively. The camera is placed 2 m away from the background scene so as to achieve balance between close and far parallax error.

The distance between the camera and the center of the mirror is supposed to be 1 m, while it is assumed that the background scene is 2 m away from the camera. As seen from the comparison between figures 5(b) and (c), the non-coated mirror reflects a much wider and more compressed area of the reverse scene than the coated mirror that magnifies the reverse scene, and more details of this scene can be observed. In other words, the coated mirror works in a similar manner as a bigger but non-coated mirror, demonstrating the magnification of scattering. This illustration indeed verifies the fact that the scattering cross section of the coated mirror is much larger than that of the non-coated one. Note that the parameters b and c can be chosen arbitrarily, although it may result in more complexity in the coating profile parameters.

4. Conclusion

We have developed a reverse methodology to realize metamaterial magnifiers in both cylindrical and spherical geometries, with the parameters simplified and evaluated. They can be reverse designed and visualized by the use of negative-index metamaterials without knowing the required spatial deformations *a priori*. The numerical results confirm the validity of the proposed concept, and also show the significance of choosing a proper generating function so as to control the field distribution pattern in the complementary media. A restriction of this method is the dependence on negative-index materials, which needs to be further investigated in future. The photorealistic rendering of an interesting magnifying metamaterial has distinct features compared to a conventional Eaton lens in terms of ray trajectories and imaging properties. This reverse transformation further allows us to efficiently optimize and simplify the magnifier's parameters by considering various $g(r)$, rather than examining a specific set of parameters calculated from a given coordinate transformation each time. The advanced photorealistic rendering developed in this paper also powers the design and evaluation in general of photonic devices.

Acknowledgments

The authors are grateful to the Temasek Defence System Institute for support through the project TDSI/11-004/1A.

References

- [1] Leonhardt U 2006 *Science* **312** 1777
- [2] Pendry J B, Schurig D and Smith D R 2006 *Science* **312** 1780
- [3] Alitalo P and Tretyakov S 2009 *Mater. Today* **12** 22
- [4] Schurig D, Mock J J, Justice B J, Cummer S A, Pendry J, Starr A F and Smith D R 2006 *Science* **314** 977
- [5] Cai W S, Chettiar U K, Kildishev A V and Shalaev V M 2007 *Nature Photonics* **1** 224
- [6] Liu R, Ji C, Mock J J, Chin J Y, Cui T J and Smith D R 2009 *Science* **323** 366–9
- [7] Lai Y, Chen H Y, Zhang Z Q and Chan C T 2009 *Phys. Rev. Lett.* **102** 093901
- [8] Yang T, Chen H Y, Luo X and Ma H 2008 *Opt. Express* **16** 18545
Luo Y, Zhang J, Chen H, Wu B I and Ran L X 2009 *Prog. Electromagnetics Res.* **95** 167
- [9] Rahm M, Cummer S A, Schurig D, Pendry J B and Smith D R 2008 *Phys. Rev. Lett.* **100** 063903
- [10] Han T, Qiu C W and Hong X 2011 *Opt. Lett.* **36** 181
- [11] Kildishev A V and Shalaev V M 2008 *Opt. Lett.* **33** 43
- [12] Chen H Y, Chan C T and Sheng P 2010 *Nature Mater.* **9** 387
- [13] Wee W H and Pendry J B 2009 *New J. Phys.* **11** 073033
- [14] Chao L, Meng X, Liu X, Li F, Fang G, Chen H Y and Chan C T 2010 *Phys. Rev. Lett.* **105** 233906
- [15] Zhang B and Barbastathis G 2010 *Opt. Express* **18** 11216
- [16] Hashemi H, Zhang B, Joannopoulos J D and Johnson S G 2010 *Phys. Rev. Lett.* **104** 253903
- [17] Zhang B, Luo Y, Liu X and Barbastathis G 2011 *Phys. Rev. Lett.* **106** 033901
Chen X, Luo Y, Zhang J, Jiang K, Pendry J B and Zhang S 2011 *Nature Commun.* **2** 176
- [18] Halimeh J C, Schmied R and Wegener M 2011 *Opt. Express* **19** 6078
- [19] Ma Y, Ong C K, Tyc T and Leonhardt U 2009 *Nature Mater.* **8** 639